FRACTOGRAPHIC PATTERNS ON FRACTURE SURFACES IN CONFINED TOUGHNESS TESTS IN SHALE ROCKS

Gonzalo Blanco[1,2], Fabián J. Antinao Fuentealba[1,2], Leandro N. Bianchi[3], Pablo Tabla[2,4], José L. Otegui[1,2], Gustavo L. Bianchi[1,2]

1: Innovation for Energy and Environment, Malvinas Institute. Faculty of Engineering, National University of La Plata, Argentina. gonzalo.blnc@gmail.com, antinao.f.j@gmail.com, jotegui60@gmail.com, gustavolbianchi@gmail.com

2: National Scientific and Technical Research Council (CONICET), Argentina. pablo.tabla@gmail.com

3: Solaer Ingeniería S.A, La Plata, Argentina. nleo.bianchi@gmail.com

4: Applied Fotonic, Faculty Regional of Delta, National Technological University (UTN-FRD), Argentina

Keywords: fracture surface, toughness, fracking, shale

RESUMEN

En este artículo presentamos caracterizaciones fractográficas cualitativas y cuantitativas de las superficies de fractura de rocas shale sometidas a ensayos de fracto-tenacidad en condiciones de presión de fondo de pozo. La tenacidad aparente a la fractura (K_{IC}) se determina en muestras cilíndricas (plugs) de 1,5" entalladas, utilizando una nueva configuración experimental. La fuerza impulsora K_I se aplica a través de un sistema hidráulico primario; un sistema hidráulico secundario e independiente aplica presiones de confinamiento de hasta 80 MPa. Las superficies de fractura se analizan mediante técnicas fotogramétricas, para descripciones cualitativas, y con un sistema de Interferometría de Baja Coherencia (LCI), para caracterizaciones cuantitativas.
Los análisis fractográficos muestran patrones distintivos bajo regímenes de propagación similares a los observados en condiciones de fondo de pozo. Se observa un efecto importante de la presión de confinamiento, tanto en los patrones en las superficies de fractura como en la fractotenacidad: las pruebas realizadas a presiones de fondo de pozo conducen a una tenacidad que duplica las de las pruebas realizadas a presión atmosférica. Los diferentes comportamientos conducen a cambios en los patrones de fractura. La presión de confinamiento, los parámetros fractomecánicos (tenacidad aparente K_{IC}, la tensión T-stress) y los parámetros fractográficos en las superficies de fractura están vinculados. Nuestros resultados muestran que la presión de confinamiento influye en el comportamiento de la fractura, lo que nos permite modelar con precisión la respuesta mecánica de las rocas shale en condiciones de reservorio.

INTRODUCTION

Characterization of rock fracability

Hydraulic fracturing is a technique to improve oil and gas hydrocarbon production from low permeability reservoirs. This method has been used and refined from 1940, and through the last 30 years it has been used in unconventional oil and gas (Smith and Montgomery, 2015). Hydraulic fracturing is a coupled hydro-mechanical process: tensile cracks are driven by high-pressure fluid injection.

Accurate characterization of rock fracability is a key issue for stimulation of unconventional reservoirs. This property controls hydraulic fracture initiation, propagation pressure and stimulated reservoir volume (SRV), which, in turn, control well productivity (Smith and Montgomery, 2015). Brittleness and its opposite, toughness, are terms used to describe rock fracability. Low fracture toughness is desirable, since it would lead to lower fracking pressures, and hence, to lower costs.

Linear elastic fracture mechanics (LEFM) have successfully predicted experimental observations for propagation of planar hydraulic fracture materials (Liu and Lecampion, 2021). However, there are some inconsistencies between laboratory results and field behavior (Liu *et al.*, 2019). Common models underestimate the observed fluid pressure and input fracture energy, and overestimate fracture length. It is recognized that the main reasonable of deviation in laboratory and field results are: I) The rock is a quasi-brittle material; a non-linear Fracture Process Zone (FPZ) forms at the fracture tip (Dutler *et al.*, 2018; Ghamgosar *et al.*, 2017). II) Higher 'apparent' toughness at field-scale, due to effects of confinement pressure and stress state anisotropy (Liu *et al.*, 2019; Mcclure *et al.*, 2020). III) apparently scale-dependent toughness in geological outcrop (Scholz, 2010), IV) Effect of surface roughness: frictional viscous losses and shear stresses (Osiptsov, 2017; Wrobel *et al.*, 2017).

Indirect field measurements of the apparent rock toughness have been made, based on injected pressure and volume records (Sampath *et al.*, 2018; Shlyapobersky and Chudnovsky, 1994). Estimates are much larger than laboratory-measured toughness values. There is still considerable uncertainty about the mechanisms that induce this toughness field stress state sensitivity, but the general concept is that as the fracture grows larger, sources of resistance to fracture propagation increase (Mcclure *et al.*, 2020).

According to the LEFM, fracture toughness K_{IC} is the main parameter to describe fracture behavior and is measured in controlled laboratory conditions. It is an intrinsic property of rock material; however, it has been shown to be dependent upon load conditions, specimen geometry, and FPZ size (Aliha *et al.*, 2018). This zone near the crack tip is subjected to damage due to high stresses and deformations; within the FPZ the fracture process eventually initiates (Dutler *et al.*, 2018).

When testing brittle materials with low tensile strength, as is the case with many rocks, it is difficult to transfer tensile forces to the samples via mechanical coupling, where the stresses are transmitted to the cracked sample from a bending moment or compression. Most samples are core-based and cylindrical: plug, disc, and half disc. Nowadays, only four specimen geometries are suggested by the International Society of Rock Mechanics (ISRM).

There is little history of tests performed under other conditions than atmospheric pressure in brittle materials (Hou *et al.*, 2016; Kataoka *et al.*, 2017; Stöckhert, 2015). Moreover, none of those techniques incorporates the effect of confinement pressure with fluid-driven opening cracks. In a recent article (Antinao Fuentealba *et al.*, 2020) the authors describe a device used to create an applied K_I through hydraulic pressure inside the notch of a cylindrical specimen, when studying natural and artificial rocks. This article describes a patented (Antinao Fuentealba *et al.*, 2020; Ramos *et al.*, 2019) procedure and experimental set up that allows carrying out fracture toughness testing in rocks, in conditions that closely match those found in the reservoir during fracking. The main original contribution of this invention lies in the devices used in actual tests of shale rocks, their use in defining the effects of confinement pressure upon the fracture toughness of shale rocks, and the methodology for statistical analysis of the results.

Propagation in brittle and quasi-brittle materials

Natural and hydraulic fractures act as transport channels for hydrocarbons. The reservoir production depends, among other factors, on the volume and conductivity of the fractures generated in the hydraulic fracture process and the proppant transport, which keep them open (Suri *et al.*, 2020; Yang *et al.*, 2022). Proppant transport and conductivity are controlled by fracture morphology, density and viscosity of the fracture fluid, proppant concentration and flow rate (Bahri and Miskimins, 2021; Roostaei *et al.*, 2018; van Dam and de Pater, 2001).

Fracture begins when the crack driving force exceeds a critical fracture energy threshold. Either stable or unstable crack propagation, this is controlled by the driving force (load or displacement controlled), and mechanisms of transport of chemical species (Atkinson, 1987; Freiman and Mecholsky, 2018). Stable propagation can be controlled by stress corrosion, and could even be insensitive to driving force, under quasi-static critical conditions. Unstable fracture is characterized by a spontaneous rupture with a high propagation rate (V_p). It can be driven by high loading rates or by overcoming critical material toughness under quasi-static loading. In this dynamic propagation regime, crack propagation speeds are in the sonic order (Ravi-Chandar, 2004).

A large number of dynamic and stable fracture propagation events (critical and sub-critical) at different geometric scales and material types have shown distinctive patterns on post-mortem fracture surfaces. In different fields of physics, engineering and geology, these patterns are referred to as “mirror”, “mist” and “hackle” (Quinn, 2016; Ravi-Chandar, 2004; Schultz, 2019). Figure

1 schematically shows these patterns: I) 'Mirror' zone: characterized by a roughly planar and clean pattern, with low roughness. It is associated with propagation initiation. II) 'Mist' zone: has a roughness greater than the previous one, and no changes are observed in growth plane, that is, Mode I prevails. III) 'Hackle' zone: roughness greater than the previous two zones, with propagation patterns that are not contained in the initial fracture plane, and possible micro-branching (i.e., small scale mixed-mode propagation).

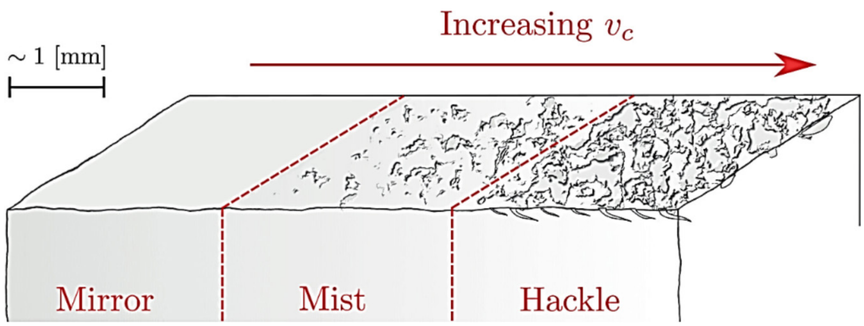

Figure 1. Distinctive patterns on post-mortem fracture surfaces. Modified after Barras (2018).

In brittle amorphous and homogeneous crystalline materials (ceramics, polymers, brittle gels) the elastodynamic LEFM predicts an increase of driving force as the propagation velocity rises, sometimes correlated with the increase in roughness (Fineberg and Bouchbinder, 2015; Ravi-Chandar, 2004; Sharon and Fineberg, 1999). In quasi-brittle materials there is no general relationship between roughness patterns and the above physical conditions. There are great difficulties in conducting experiments on these materials: energy dissipation mechanisms in FPZ are nonlinear and intrinsic heterogeneities continuously modify the stress field as the fracture evolves (Bonamy and Bouchaud, 2011).

Recent research show that fracture surface roughness has an important impact in proppant transport. Fractures with rougher surfaces cause turbulent flows, this turbulence increases horizontal velocity of proppant transport and its capacity to remain in suspension. These allow it to reach greater distances in the generated fractures, improving the permeability of the reservoir (Suri *et al.*, 2020; van Dam and de Pater, 2001; Zhang *et al.*, 2019).

Fracture characterization techniques in the field include microseismic (Maxwell, 2014), fiber optics (Jin and Roy, 2017; Karrenbach *et al.*, 2017), pressure and temperature sensing (Spicer and Coenen, 2018; Webster *et al.*, 2013) and electromagnetic images (Li and Yang, 2021). All these techniques characterize the geometry of the generated fracture network, but none of them give us information about the fracture morphology. Currently, there is a lack of in-situ methods to determine the morphological characteristics of the fracture surface. In this work, we present a qualitative and quantitative characterization of fracture surface generated in a hydraulic fracturing test under downhole conditions at laboratory scale. The tests were carried out under confining pressures up to 70 MPa (10000 psi). Moreover, we resort to low coherence laser interferometry (LCI) test as an optical technique to study these surfaces, since it is very versatile and a high-resolution technique (Cerrotta *et al.*, 2015; Morel *et al.*, 2018). The samples used are outcropping rocks corresponding to the upper carbonatic layer of the Vaca Muerta formation. The typical pressures of this formation range from 55 to 70 MPa (Frydman *et al.*, 2016; Sánchez Camus *et al.*, 2021).

EXPERIMENTAL METHODS AND RESULTS

Rock toughness testing

The novel testing device used for measuring Mode I rock toughness (K_{IC}) has been presented in recent articles (Antinao Fuentealba, *et al.*, 2020; Antinao Fuentealba *et al.*, 2020). This device allows measure K_{IC} under stress triaxiality and temperature conditions similar to those at a shale-type hydrocarbon reservoir allows determining rock toughness via simultaneously applying pressures:

1. inside a pre-existing crack, by pumping various fracture fluids at inner pressure Pi (inner device, part 5 in Fig. 2). As discussed in (Antinao Fuentealba *et al.*, 2020), the device uses a cylindrical specimen (plug), with a straight or chevron notch. The load is transmitted by applying pressure on notch surfaces.
2. in a vessel enclosing the previous device, where pressure and temperature are maintained with another (outer) fluid, matching well bottom conditions, up to 90°C and 80 MPa, (part 4, Fig. 2).

The outer vessel holds the triaxial confinement pressure, Pc. Its main components are indicated in the scheme of Fig. 2. The vessel (4) is bolted to a flat closing plate containing the conduits that transmit both pressurized fluids (internal and confinement), and signals from temperature and pressure sensors. Pressures Pi and Pc are regulated by a system of piston-cylinder and screw compressors (7-8). Fig. 2 (4-5) shows both pressure chambers: the inner pressurizing device (Pi), and the confinement pressure vessel (Pc). Operating pressures are large (up to 80 MPa). In the inner device a pressure Pi is applied, that exceeds Pc, so that the crack growth driving force is proportional to P:

$$P = P_i - P_c \quad (1)$$

The low cost of specimen machining and testing allows obtaining many results for the same condition at an affordable cost, thus facilitating performing multiple validation tests and further reducing the uncertainties inherent to these experimental measurements.

Samples of the order of a cubic foot are extracted from the outcrops of the formation (Antinao Fuentealba *et al*., 2020). Cylindrical plugs or samples are machined using a diamond drilling cup. Diffraction Ray X (DRX) results show that rocks have mainly high contents of calcite (89%) and quartz (10%), with clays percentage lower than 1% (smectite and feldspar).

Plugs are 38 mm (1 1/2”) in diameter and around 60 mm long. From one to three notches are then machined with diamond wire, making sure that notch surfaces are planar and perpendicular to the plug axis, rock lamination, and weak planes (Fig. 3A). The multi-notched plug allows large sampling of fracture toughness data with low cost and manufacturing time. The tests are always performed one notch at a time. The specimens are dried for 24 hours (dry condition). Then varnish is applied to prevent incorporation of room moisture and to ensure proper sealing in the inner device.

Once the plug is placed in the inner device and the outer vessel is bolted in place, the fracture fluid (water) and confinement fluid (water-based lubricant) are injected simultaneously. The loading time were nearby 10-20min. Once the desired confinement pressure is reached, pressure in the inner device is increased until the specimen fractures. It was done 44 fracture toughness tests in dry conditions, notch ratio $0.08 < a/D < 0.25$. As it shows in (Antinao Fuentealba *et al*., 2020), fracture toughness is sensitive to notch ratio.

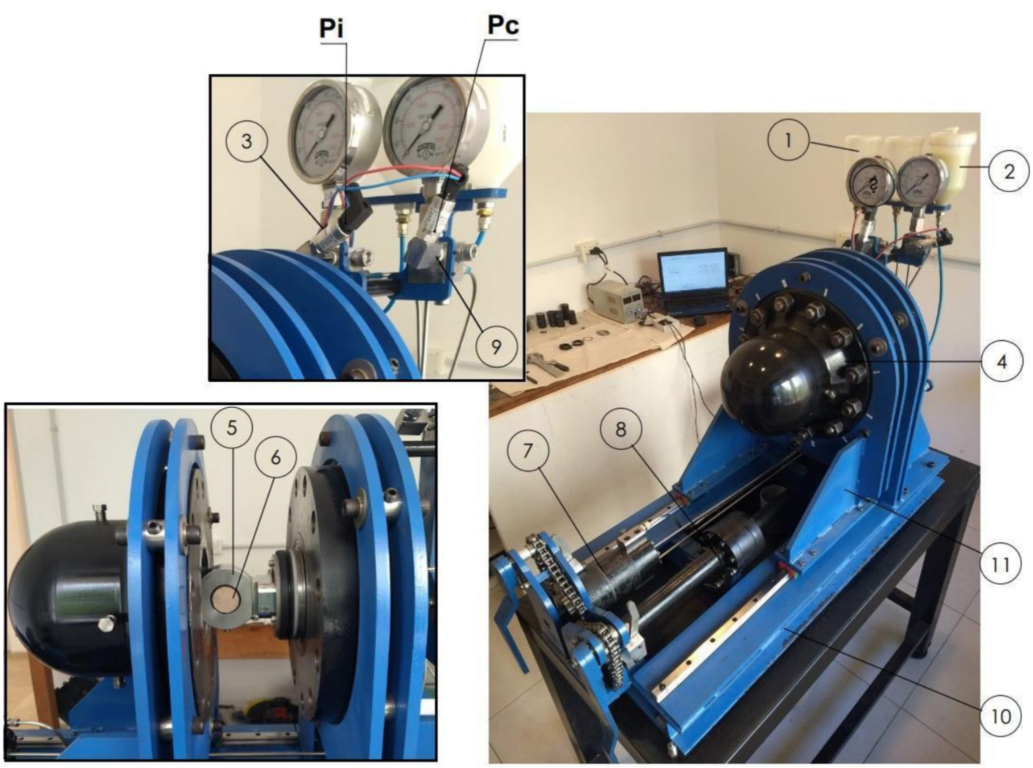

Figure 2. External view of the test machine. Constructive and operational aspects of both pressure chambers are shown. Main parts: (1-2) Inner and outer fluid repositories, (3-9) Manifold and pressure transducer P_i and P_c, (4) Confinement pressure vessel (Pc), (5) Inner pressure chamber, (6) Rock sample, (7- 8) Pressure intensifier for inner and outer fluids, (10) Fixed base, (11) Mobile base. From Antinao Fuentealba *et al*. (2020).

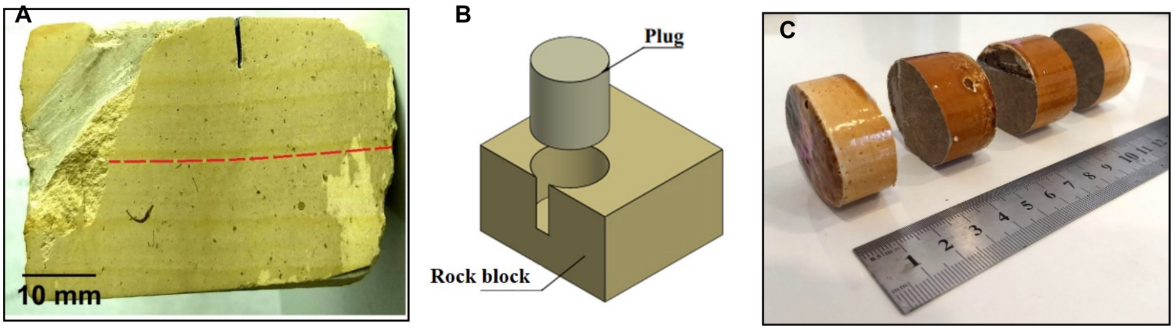

Figure 3. a) Relative direction of rolling planes and crack planes. b) Machining of cylindrical plugs or specimens. c) Specimens broken after toughness tests. Modified after Antinao Fuentealba *et al.* (2020).

Rock toughness measurements

A recent article shows that the fracture toughness under confining pressure by using round bar specimen, can be calculated by expression (2) and (3) the time of rupture at pressure P (Antinao Fuentealba *et al.*, 2022):

$$K_{IC} = P\sqrt{\pi\, a}\, F(a/D) \tag{2}$$

where a is notch depth and D is diameter of specimen, and F is a function that depends on sample geometry. This factor was calibrated by using finite element models, and eq. 3 is valid for notch ratio 0.1<a/D<0.25.

$$F\left(\frac{a}{D}\right) = 0.638 + 2.45\left(\frac{a}{D}\right) - 0.637\left(\frac{a}{D}\right)^2 \tag{3}$$

K_{IC} results for specimens under confinement pressure and temperature close to 3000 m deep well bottom conditions in the carbonatic upper layer of Vaca Muerta oil and gas reservoirs are shown in Figure 4. As it is shown in (Antinao Fuentealba *et al.*, 2020), toughness results are sensitive to notch ratio a/D. It is observed that with a confinement pressure of 70 MPa the estimated apparent toughness values are two times those measured under atmospheric conditions.

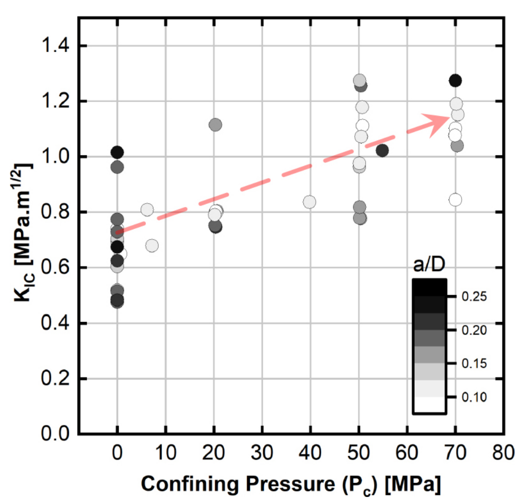

Figure 4: Fracture toughness results for Vaca Muerta carbonatic rock in dry conditions for different confinement pressures.

Qualitative fractographic analysis

Figure 5 shows the fractographic patterns of fracture some surfaces. Numbers I, II and III indicate confinement pressures: 0, 20 and 50 MPa, respectively. A clear evolution of surface patterns with confinement pressure is observed. At low pressure, no distinctive pattern is detected. At middle and high pressures, flattened ("mirror") zones are localized near the initial notch. The size of the mirror zone tends to be larger as pressure increases from mid to high. In accordance with fractographic and dynamic fracture literature (Hull, 1999; Quinn, 2016; Ravi-Chandar, 2004), the observed patterns are consistent with a dynamic cracking regime. After reaching the peak-load, the propagation is unstable and the crack tip probably growths at near sonic velocities.

Figure 5. Evolution of fracture surface against confinement pressure. The notation I, II and III correspond to atmospheric condition, 20-30 and 50 MPa respectively. The arrows indicate approximate position of mirror zone.

The qualitative characterization of the fracture surfaces was carried out through the sample observation and photographic images by lighting the sample from different angles to enhance its morphological characteristics, by using an optical microscope. This allowed to differentiate three zones (Fig. 6):

- Initiation Zone (ZI): surface close to the notch, it is the area with less roughness associated whit the typical "mirror zone".
- Transition Zone (ZT): this arear exhibits a gradual increase in roughness as it moves away from the notch.
- Propagation Zone (ZP): is the farthest area from the notch. It has greatest of roughness.

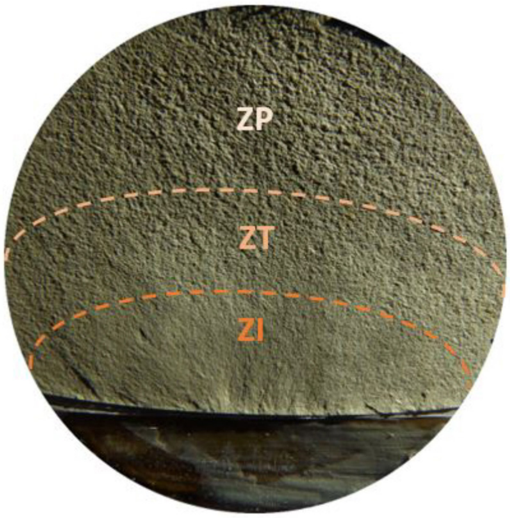

Figure 6. Fracture surface zones. Zone ZI is the initiation zone near to the main crack, Zone ZT is the transition zone, and the zone ZP is the farthest area from the notch. Dotted lines delimit each zone.

Quantitative fractographic testing

To quantify the changes in the fracture surfaces, roughness parameters are estimated from a height map obtained with an optical equipment based on low coherence laser interferometry (LCI). The LCI is a high-resolution, non-destructive optical technique that uses a light source with a wide spectral width that is focused on a point on the sample to determine the depth distance between this point and a reference surface. The Michelson interferometer is the traditional experimental scheme for this technique. In the present study, a configuration based on optical fiber and with a single branch is used, with the aim of improving the signal-to-noise ratio (Fig. 7).

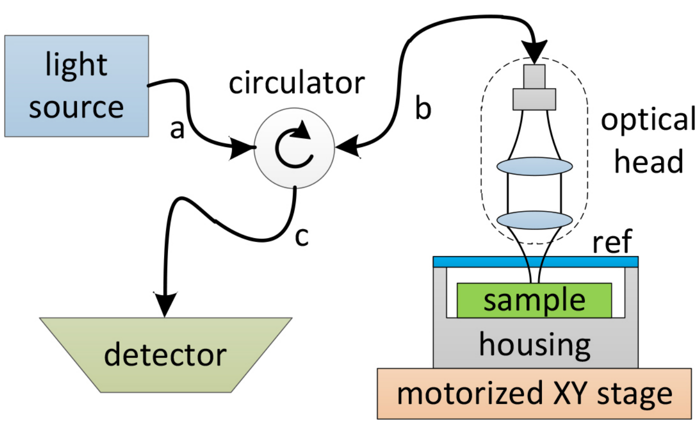

Figure 7. Scheme of the interferometer system of a single branch based on fiber optics.

The light emitted by the source travels through the set of optical fibers a and b, to the optical head that focuses the beam on the sample and on the reference window. The generated reflections are collected by the same optical head and sent to the detector (spectrometer) through fibers b and c. The positioners are two DC motors arranged in the plane normal to the optical axis (XY plane) and move the sample together with the reference surface and the support to measure the sample of interest point by point and reconstruct the 3D image (Fig. 8).

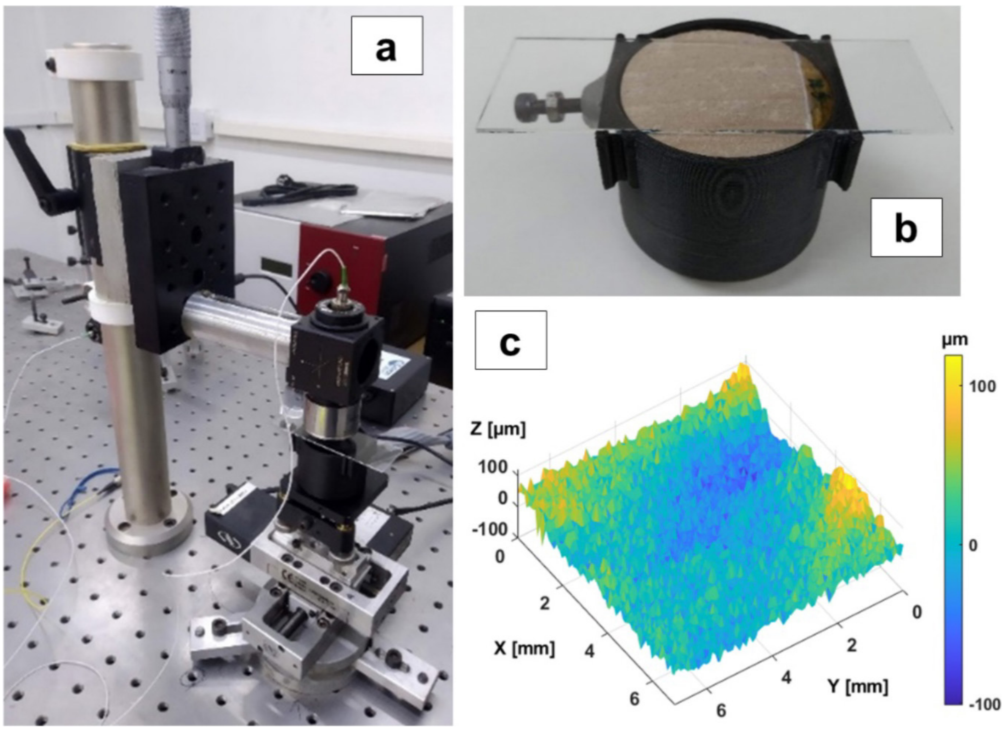

Figure 8. a) Optical test device. b) Specimen placed in the sample holder, ready to be tested. c) Height map of the fracture surface resulting from the optical test.

The optical tests were carried out with an axial resolution of about 5 um and 100 µm in the horizontal plane. They were limited to mapping a representative area of each zone of interest (ZI, ZT and ZP). These areas were selected far enough from the sample edges because of the loss of stress triaxiality state due to the decrease in material between the crack tip and the sample edges as the crack propagates.

Figure 9 shows the height map of each study area from Figure 6, obtained by optical measurement. Both ZI and ZP areas have a size of 7 mm x 7 mm (4900 measured points) and ZP has an area of 10mm x 2mm (2000 measured points).

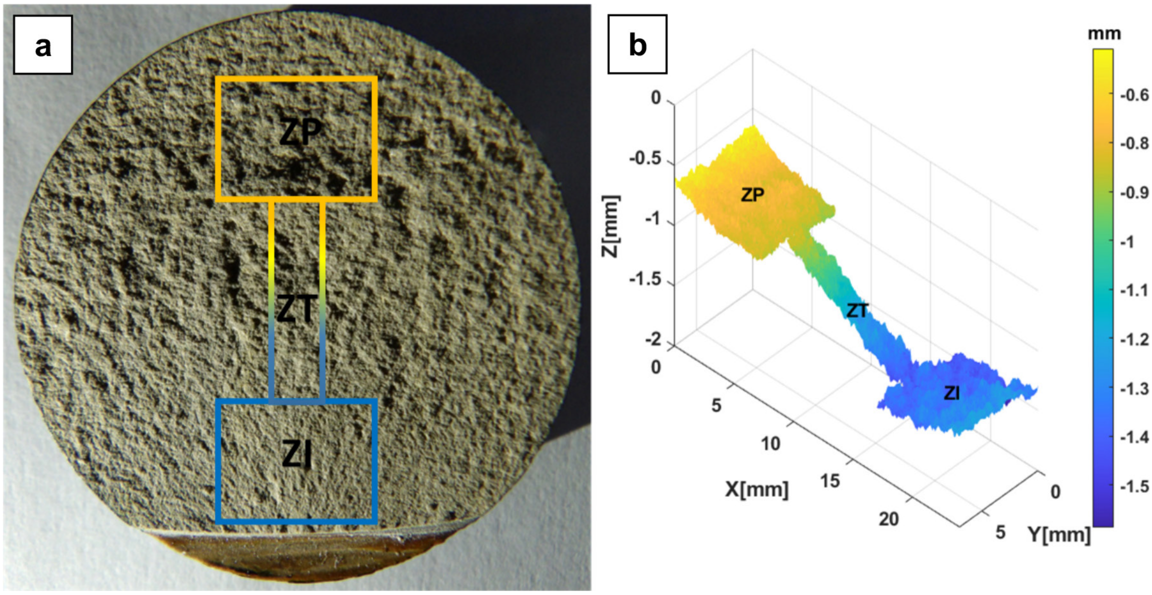

Figure 9. a) Sample and the tested area. b) Height map as resulting of tested area.

Quantitative fractographic analysis

There are different parameters to quantify the surface roughness. These can be classified into three groups: statistical, fractal and directional parameters (Magsipoc *et al.*, 2020; Yang *et al.*, 2022). In this work we determine two statistical parameters directly from the fracture surface height map, without the need to perform any advance processing technique beyond the general ideas of statistics.

- The arithmetic average of the absolute height (Ra)

$$Ra = \frac{1}{nm}\sum_{i=1}^{n}\sum_{j=1}^{m}|Z_{ij}| \tag{2}$$

- The root mean square of height (Rq)

$$Rq = \sum_{i=1}^{n}\sum_{j=1}^{m}\sqrt{\frac{Z_{ij}^2}{nm}} \tag{3}$$

Where n and m are the number of points on the X and Y directions, and Z_{ij} is the height of the point in the i-j-th position respect to a reference surface. These are the simplest and general parameters for roughness characterization. Both parameters measure the relative deviation of surface from the mean plane of the surface, and they are very close numerically (Magsipoc *et al.*, 2020; Yang *et al.*, 2022).

The optical tests were carried out on 21 samples, testing at different confining pressure (0, 20, 50 and 70 MPa) and notch ratios $0.1 < a/D < 0.25$. After performing the optical tests, the data is processing following the next sequence:

1. Through a cut-off value, any point measured out of range is eliminated and a new value of height obtained from a simple average of the eight closest points is reassigned. They are easily observable because, generally, differ from the rest of measured points in, at least, one order of magnitude (Fig. 10 a.
2. The horizontal fracture surface (HFS) is determined by subtracting from each area of interest (ZI, ZT and ZP) its mean plane determined by the method of least squares (Fig. 10 b). This new surface is the one that contains all the roughness information (Fig. 10 c). This procedure is necessary because mode l propagation hypothesis is supposed and also to eliminate any type of inclination in the fracture surface generated in the optical test due to an incorrect placement of the plug in the sample holder, causing the direction of the laser light beam to not be normal to the fracture surface.
3. Estimation of roughness parameters from each HFS.

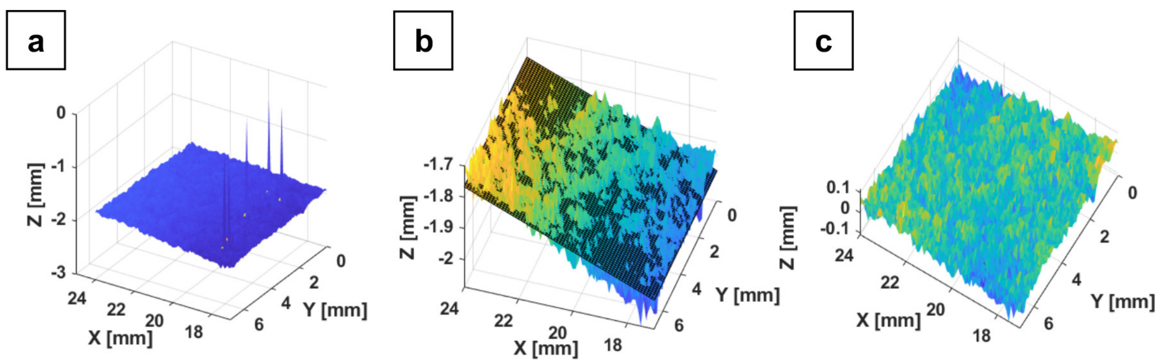

Figure 10. Data processing sequence. a) Height map resulting from the optical test, without filtering. b) Height map after cut-off filter applied and its mean plane (black). c) Horizontal fracture surface.

Figure 11 shows two scatter plots of roughness parameters for the entire sample as a function of the confining pressure and toughness, without separating the three distinctives zones (ZI, ZT and ZP). The gray levels reflect the toughness of the sample according to Figure 4.

It is observed that the general roughness of the fracture surfaces decreases as the confining pressure increases. Also, for confining pressure of 20 and 70 MPa, the roughness parameters decrease with increasing in toughness. This trend is not observed for tests at 50 MPa of confining pressure. It is argued that due to weathering effects. The outcrop rock extracted for the tests at this confining pressure was the most superficial and therefore the one most likely to be affected. If that is true, part of the block could present a decline in its mechanical parameters that would affect the roughness of the fracture surface. Another hypothesis for this behavior could be founded in unequal chemical composition, geological history, and heterogeneities between rock blocks. As shown Figure 4, this is reflected in the scatter of fracture toughness values. The heterogeneities generate a non-uniform stress distribution (stress anisotropy), that modifies local stress states at all scales.

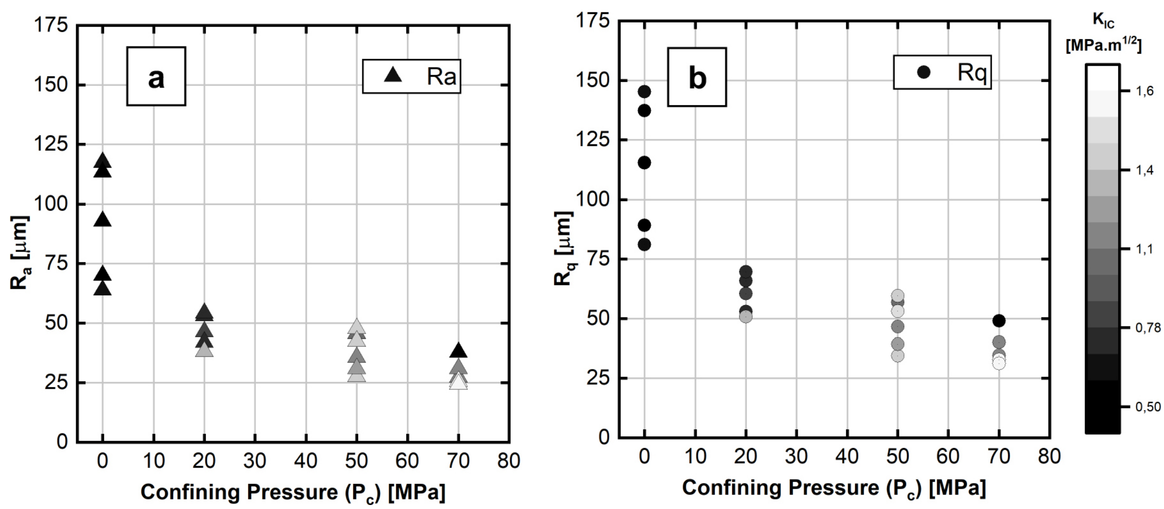

Figure 11. Roughness parameters R_a (a) and R_q (b) of the entire sample as a function of the confining pressure and toughness (gray level).

From the roughness parameters obtained for each sample, a simple average was calculated for each confinement pressure, obtaining a representative value of R_a and R_q for each pressure (Fig. 12). These results clearly show the decrease in roughness with confining pressure. The most notable change occurs between the tests at 0 MPa and 200 MPa, since the roughness values decrease by half.

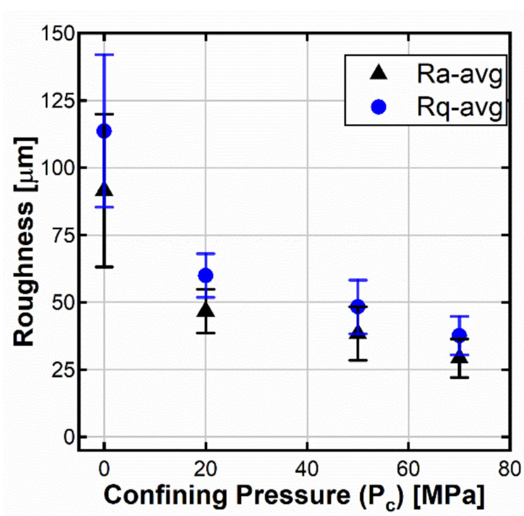

Figure 12. Average of roughness parameters R_a (black) and R_q (blue) and its standard deviation for each confining pressure.

Figure 13 shows the results of the analysis performed for ZI and ZP individually. Aiming to obtain a representative value of roughness for each area of interest at different confining pressures, the average roughness parameters were estimated for the individual zones in all specimens. For both ZI and ZP a quasi-linear decrease in the average roughness is observed as confining pressure increases. Also, the roughness parameters of ZI are lower than the roughness parameters for ZP at the same confinement.

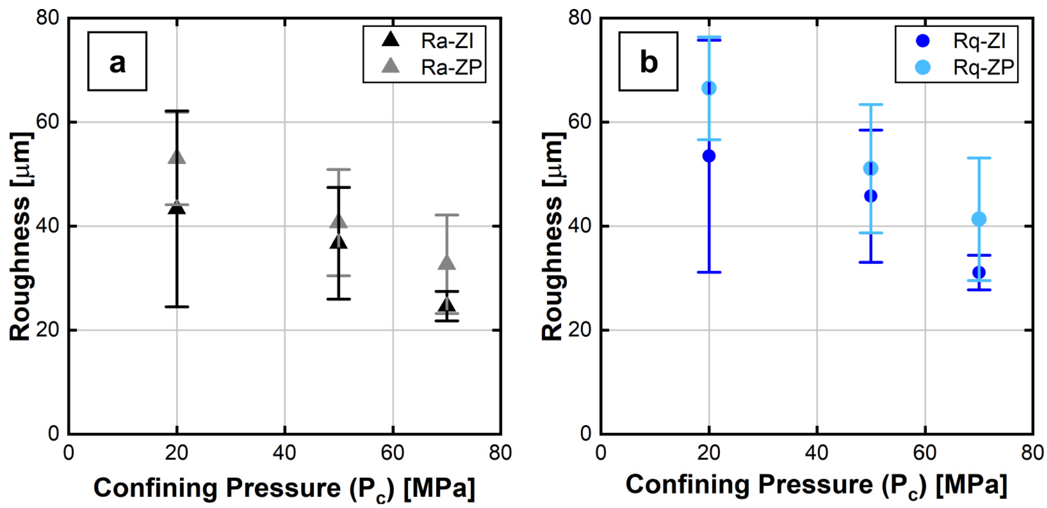

Figure 13. Average of roughness parameters R_a (a) and R_q (b) and its standard deviation for each confining pressure for ZI and ZP.

DISCUSSION

Extracting meaningful data from surface fractures is a topic of various domains of physics and engineering. In rock mechanics, rock fracture surfaces may show multiple-scale patterns, from geological (Sagy *et al.*, 2001; Savalli and Engelder, 2005) to laboratory scale (Ougier-Simonin *et al.*, 2016; van Dam and de Pater, 2001; Zhang and Zhao, 2014). However, scarce research has been devoted to rock fracture, probably due to technical and experimental difficulties related to heterogenies and the non-lineal behavior (Zhang and Zhao, 2014).

Our experimental results confirm that rock fracture toughness and fracture surface roughness strongly depend upon confinement pressures. In well bottom conditions apparent toughness values are up to two times those measured under atmospheric conditions. This is a non-conservative result, as it leads to underestimating pressures required for fracking during the stimulation of unconventional reservoirs. In accordance with the conceptual and empirical behavior of fracture toughness, it is shown that for grater confinement pressure, larger fracture resistance. It remains uncertain the mechanisms that induce this behavior, however, it is suggest that triaxial state quantified by multi-parameter fracture toughness approach (K, T-stress, and other non-singular parameters) could be useful to explain the results (Hou *et al.*, 2021).

Under zero triaxiality conditions, there is no characteristic pattern on fracture surfaces, which show a homogeneous roughness. At medium and high confinements (20-50-70MPa) a gradual transition in fractographic patterns is evident. Characteristic fractography patterns have been identified in brittle materials (Gale *et al.*, 2018; Nakamura *et al.*, 2020; Raterman *et al.*, 2019): mirror-mist-hackle transitions. As seen in Figure 6, an increase in roughness from the mirror area is observed in our tested specimens as the degree of confinement increases. The roughness parameters decrease gradually from 0 to 70 MPa. The most significant variation in roughness occurs between zero triaxiality condition and the confining pressure of 20 MPa. Parameters R_a y R_q decreased almost by half, around 50-60 um. Then, as the confining pressured increased, the roughness continuously decreased (Fig. 12). Fractographic patterns are a direct consequence of the evolution of the FPZ during propagation, therefore propagation rate regimes are dependent upon confinement pressure. Once the maximum load was reached in our tests, propagation became unstable and high crack growth developed. Thus, the identified patterns are characteristic of the dynamic crack growth regime.

It is noticed that field observation and experimental laboratory data do not confirm the propagation velocity regimes and roughness patterns correlation. Both dynamic and quasistatic regimens can also generate these morphologies. Field models and estimates show that crack propagation rates are in the order of 1–10 m/s (Bahat *et al.*, 2005; Fineberg and Bouchbinder, 2015; Zhang and Zhao, 2014). That is, two orders of magnitude lower than the characteristic speeds in the dynamic regime. On the other hand, mirror-mist patterns have been found in geological formations, with estimates of subcritical speeds in the order of 10-7 – 10-2 m/s (Antinao Fuentealba *et al.*, 2018). In addition, empirical evidence found in well bottom cores shows an evolution of overall flat fractures (10 m scale), that on a small scale show complex fracture patterns (10-1 m scale). Characteristic patterns of dynamic evolution have been found on these scales so that uncertainties regarding propagation regimes continue.

It has been hypothesized that the success of hydraulic stimulation in unconventional formations is dependent upon the creation of a 'complex network' (Mcclure *et al.*, 2020). Under this approach, propagating hydraulic fractures frequently terminate against natural fractures, creating a branching and 'complex' network of both new and preexisting fractures. Those interactions take place under different propagation regimes. The degree of surface roughness can be related to the mechanism of reservoir enhancement-permeability. Thus, the more roughness in surfaces, the more likely is the tendency to complex fracture.

Recent core analysis from bottom-hole fracture observations have shown considerable small-scale complexity, even though the fractures appear to be approximately planar at field-scale (Gale *et al.*, 2018; Raterman *et al.*, 2019). Figure 14 shows some features on the fracture surfaces of cores, such as mist-hackles and plumose/mirror markings, that correlate with propagation direction and initiation of global planar fracture. Thus, there is no consensus about the mechanisms of fracture propagation and enhanced-permeability in unconventional reservoir.

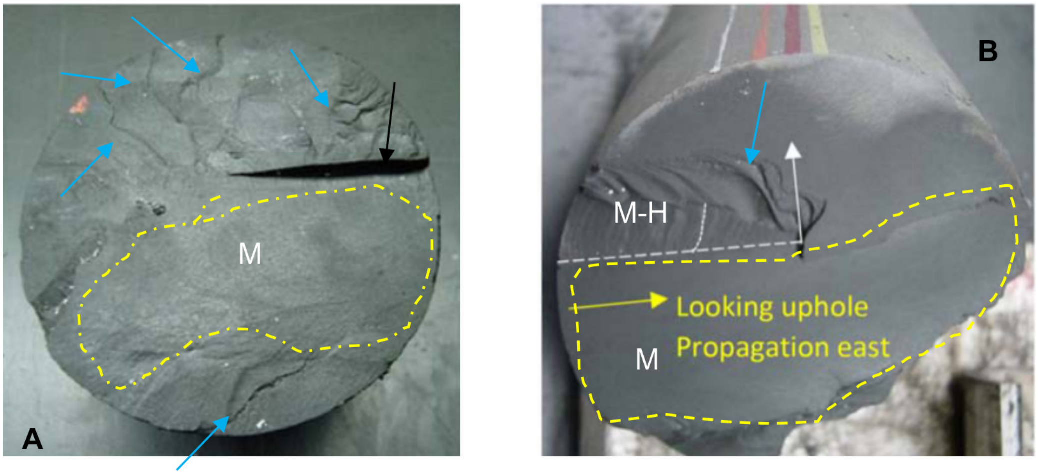

Figure 14. Examples of surface morphology in hydraulic fracture core: a-b) Mirror (M, yellow zone) and mist-hackle pattern (M-H, light blue arrows) and interaction with weakness-plane (black arrow). B) Local direction of growth is normal to that line (white arrow). Overall fracture propagation direction given by yellow arrow. Modified after Gale *et al.*, (2018).

Hydraulic fracture experiments made with synthetic and diatomite rock under different stress triaxiality conditions in the quasi-static propagation regime show "mirror-mist-hackle" patterns, with roughness dependence upon confinement pressure and material (van Dam and de Pater, 2001). It is argued that near FPZ the triaxial stress state can be compatible with shear failure. The hackle-branching patterns are due to weakening induced from shear failure inside the FPZ. During quasi-static propagation, there is energy consumption from surface creation along the mode I plane, but microcracks dissipate energy near the FPZ in other aleatory directions. These intrinsic defects could allow tilt and twisting of the crack tip front, i.e, micro-branching. This explanation is supported by another research (Ravi-Chandar, 2004).

In laboratory-scale, the influence of confining pressure could be captured by the first non-singular parameter of the William's series near the crack tip, the T-stress parameter, which is recognized in rock fracture mechanics (Mirsayar *et al.*, 2018). The theory states that in quasi-static regime, T-stress causes deviation of the crack path from the mode I fracture plane, while in dynamic fracture there is still a degree of uncertainty (Gupta *et al.*, 2015). Recent articles (Kawabata *et al.*, 2019; Nakamura *et al.*, 2020) show experiments in the dynamic fracture regime, using bending and tensile steel specimens. Correlation between measured propagation velocities, physical position of fractographic patterns and triaxiality level (T-stress), allowed identifying a criterion for crack patterns: macro-branching is promoted by high triaxiality stress levels. However, this hypothesis is still not quantified in rocks.

In our experiments, confinement controls fracture toughness and propagation speeds once fast crack growth. Therefore, confinement also controls fractographic patterns. Recent research emphasizes the incorporation of apparent toughness into physical models as well as the effects of heterogeneity, roughness (shear stress, friction losses). In any case, more research is needed in order to better determine the relationship between triaxiality and surface roughness patterns on post-mortem specimens.

CONCLUSIONS

The inconsistencies between laboratory-scale experiments, proposed physical models, and field evidence make it difficult to optimize hydraulic fracturing operations in oil and gas fields, and therefore their economic feasibility. This paper discusses the use of a linear elastic fracture mechanics approach based on the critical crack-tip stress intensity factor (K_I) to characterize rock fracability under real well bottom conditions.

A novel experimental set up has been used, in which the mode-I crack driving force (K_I) is applied by means of a hydraulic pressure inside the crack, so that fracturing fluid chemistry can be modified. A secondary hydraulic system ensures variable confinement pressures, up to 80 MPa. Also, post-mortem fracture surfaces were analyzed by an optical test device.

Fracture Toughness (K_{IC}) and roughness parameters are determined in notched 1.5” plugs machined from rocks, which can be re-used several times and require much less material than standard Brazilian discs and semicircular three-point bending specimens. Experimental assessment of the effect of confinement pressure upon rock fracture toughness is discussed in terms of K_{IC} measurements conducted on rock samples. A major effect of confinement pressure is observed: tests carried out at well-bottom pressures lead to apparent rock toughness doubling those for tests carried out at atmospheric pressure.

From the qualitative analysis of the fracture surfaces, 3 distinctive zones were found. The results from the optical test based on LCI confirm what was observed in the qualitative analysis, allowing us to ensure that this technique is valid for the characterization of roughness in geological samples. The maximum value in roughness was observed for test under no confining pressure with a roughness value around 100 um. As the confining pressure of the test increased, the roughness decreased. For Vaca Muerta pressures of 50 MPa (oil window) the roughness was around 45 um and for the gas window, with typical pressures near to 70 MPa (10,000 PSI), it was close to 35 um.

These results show that increasing triaxial pressure confinement allows to accurately model the mechanical response of shale rocks in actual reservoir conditions and add information about the morphology of fracture surface.

REFERENCES

Aliha, M. R. M., Mahdavi, E. and Ayatollahi, M. R., 2018. Statistical Analysis of Rock Fracture Toughness Data Obtained from Different Chevron Notched and Straight Cracked Mode I Specimens. Rock Mechanics and Rock Engineering, 51(7), 2095–2114

Antinao Fuentealba, F. J., Bianchi, G. L., Sánchez Camus, A. and Ramos, R., 2018. Fracture toughness experiments in shale rocks, effect of fluid chemestry on KIc. 10th Hydrocarb. Explor. Dev. Congr., 1–17.

Antinao Fuentealba, F. J., Bianchi, L. N., Otegui, J. L. and Bianchi, G. L., 2022. Accurate experimental determination of rock fracture toughness under simulated reservoir confining. Sent to Theoretical and Applied Fracture Mechanics.

Antinao Fuentealba, F. J., Otegui, J. L. and Bianchi, G. L., 2020. Improved technique for toughness testing of shale rocks. Engineering Fracture Mechanics, 235(June), 13.

Antinao Fuentealba, F. J., Romero, J. J., Otegui, J. L. and Bianchi, G. L., 2020. Device for rock fracture toughness testing under hydrocarbon reservoir conditions. Theoretical and Applied Fracture Mechanics, 109(July), 102718.

Atkinson, B. K., 1987. Fracture mechanics of rock. Academic Press.

Bahat, D., Rabinovitch, A. and Frid, V., 2005. Tensile Fracturing in Rocks. Springer-Verlag Berlin Heidelberg.

Bahri, A. and Miskimins, J., 2021. The Effects of Fluid Viscosity and Density on Proppant Transport in Complex Slot Systems. SPE Production and Operations, 36(4), 894–911.

Barras, F., 2018. When dynamic cracks meet disorder: A journey along the fracture process zone. Ecole Polytechnique Fédérale de Lausanne (EPFL).

Bonamy, D. and Bouchaud, E., 2011. Failure of heterogeneous materials: A dynamic phase transition? Physics Reports, 498(1), 1–44.

Cerrotta, S., Morel, E. N. and Torga, J. R., 2015. Scanning Optical Coherence Tomography Applied to the Characterization of Surfaces and Coatings. Procedia Materials Science, 9, 142–149.

Dutler, N., Nejati, M., Valley, B., Amann, F. and Molinari, G., 2018. On the link between fracture toughness, tensile strength, and fracture process zone in anisotropic rocks. Eng. Fract. Mech., 201, 56–79.

Fineberg, J. and Bouchbinder, E., 2015. Recent developments in dynamic fracture: some perspectives. International Journal of Fracture, 196(1–2), 33–57.

Freiman, S. W. and Mecholsky, J. J., 2018. The Fracture of Brittle Materials. In The American Ceramic Society (Ed.), The Fracture of Brittle Materials (2nd ed.). Wiley.

Frydman, M., Pacheco, F., Pastor, J., Canesin, F. C., Caniggia, J. and Davey, H., 2016. the SPE Argentina Exploration and Production of Unconventional Resources Symposium.

Gale, J. F. W., Elliott, S. J. and Laubach, S. E., 2018. Hydraulic fractures in core from stimulated reservoirs: Core fracture description of HFTs slant core, Midland Basin, West Texas. SPE/AAPG/SEG Unconventional Resources Technology Conference 2018, URTC 2018, 1993.

Ghamgosar, M., Erarslan, N. and Williams, D. J., 2017. Experimental Investigation of Fracture Process Zone in Rocks Damaged Under Cyclic Loadings.

Experimental Mechanics, 57(1), 97–113.

Gupta, M., Alderliesten, R. C. and Benedictus, R., 2015. A review of T-stress and its effects in fracture mechanics. Engineering Fracture Mechanics, 134, 218–241.

Hou, C., Wang, Z., Jin, X., Ji, X. and Fan, X., 2021. Determination of SIFs and T-stress using an over-deterministic method based on stress fields: Static and dynamic. Engineering Fracture Mechanics, 242(July 2020), 107455.

Hou, C., Wang, Z., Liang, W., Li, J. and Wang, Z., 2016. Determination of fracture parameters in center cracked circular discs of concrete under diametral loading: A numerical analysis and experimental results. Theoretical and Applied Fracture Mechanics, 85, 355–366.

Hull, D., 1999. Fractography: Observing, Measuring and Interpreting Fracture Surface Topography. Cambridge University Press.

Jin, G. and Roy, B., 2017. Hydraulic-fracture geometry characterization using low-frequency DAS signal., 36(12), 975–980.

Karrenbach, M., Ridge, A., Cole, S., Boone, K., Kahn, D., Rich, J., Silver, K. and Langton, D., 2017. DAS microseismic monitoring and integration with strain measurements in hydraulic fracture profiling. SPE/AAPG/SEG Unconventional Resources Technology Conference 2017.

Kataoka, M., Mahdavi, E., Funatsu, T., Takehara, T., Obara, Y., Fukui, K. and Hashiba, K., 2017. Estimation of Mode i Fracture Toughness of Rock by Semi-Circular Bend Test under Confining Pressure Condition. Procedia Engineering, 191, 886–893.

Kawabata, T., Tonsho, F., Nishizono, Y., Nakamura, N. and Takashima, Y., 2019. Controlling factors for roughness increases on cleavage fracture surfaces and crack branching in polycrystalline steel. Theoretical and Applied Fracture Mechanics, 100(January), 171–180.

Li, Y. and Yang, D., 2021. Electrical imaging of hydraulic fracturing fluid using steel-cased wells and a deep-learning method.1, 86(4), E315–E332.

Liu, D. and Lecampion, B., 2021. Propagation ofa plane-strain hydraulic fracture accounting for a rough cohesive zone. Journal of the Mechanics and Physics of Solids, 149(January), 104322.

Liu, D., Lecampion, B. and Garagash, D. I., 2019. Propagation of a fluid-driven fracture with fracture length dependent apparent toughness. Engineering Fracture Mechanics, 220(May), 106616.

Magsipoc, E., Zhao, Q. and Grasselli, G., 2020. 2D and 3D Roughness Characterization. Rock Mechanics and Rock Engineering, 53(3), 1495–1519.

Maxwell, S., 2014. Microseismic Imaging of Hydraulic Fracturing. In Microseismic Imaging of Hydraulic Fracturing. Society of Exploration Geophysicists.

Mcclure, M., Picone, M., Fowler, G., Ratcliff, D., Kang, C., Medam, S. and Frantz, J., 2020. Nuances and Frequently Asked Questions in Field-Scale Hydraulic Fracture Modeling Data-driven and physics-based models. SPE-199726-MS, 1, 1–19.

Mirsayar, M. M., Razmi, A., Aliha, M. R. M. and Berto, F., 2018. EMTSN criterion for evaluating mixed mode I/II crack propagation in rock materials. Eng. Fract. Mech., 190, 186–197.

Morel, E., Torga, J. R., Tabla, P. M. and Sallese, M., 2018. Reduction of measurement errors in OCT scanning.

Nakamura, N., Kawabata, T., Takashima, Y. and Yanagimoto, F., 2020. Effect of the stress field on crack branching in brittle material. Theoretical and

Applied Fracture Mechanics, 108(October 2019). https://doi.org/10.1016/j.tafmec.2020.102583

Osiptsov, A. A., 2017. Fluid Mechanics of Hydraulic Fracturing: a Review. Journal of Petroleum Science and Engineering, 156(May), 513–535.

Ougier-Simonin, A., Renard, F., Boehm, C. and Vidal-Gilbert, S., 2016. Microfracturing and microporosity in shales. Earth-Science Reviews, 162, 198–226.

Quinn, G. D., 2016. NIST Recommended Practice Guide Fractography of Ceramics and Glasses (NIST, Ed.; 2nd ed.).

Ramos, R., Antinao Fuentealba, F. J., Bianchi, G. L., Otegui, J. L. and Romero, J. J., 2019. Device for experimental measurement of fracture toughness of rocks in hydrocarbon reservoir conditions. Argentine National Institute of Industrial Property (INPI), Act No. 20190103453, 2019. Patent pending.

Raterman, K. T., Liu, Y. and Warren, L., 2019. Analysis of a drained rock volume: An eagle ford example. SPE/AAPG/SEG Unconv. Resour. Technol. Conf. 2020, URTeC 2020, 1–20.

Ravi-Chandar, K., 2004. Dynamic Fracture. In Dynamic Fracture. Elsevier Ltd.

Roostaei, M., Nouri, A., Fattahpour, V. and Chan, D., 2018. Numerical simulation of proppant transport in hydraulic fractures. Journal of Petroleum Science and Engineering, 163, 119–138.

Sagy, A., Reches, Z. and Roman, I., 2001. Dynamic fracturing: Field and experimental observations. Journal of Structural Geology, 23(8), 1223–1239.

Sampath, K. H. S. M., Perera, M. S. A. and Ranjith, P. G., 2018. Theoretical overview of hydraulic fracturing break-down pressure. Journal of Natural Gas Science and Engineering, 58(August), 251–265.

Sanchez Camus, A. A., Ramos, R. and Rotili, C., 2021. Integral characterization of the Vaca Muerta formation. 3D numerical modeling of the complete cycle of vertical well located in the oil generation window. 55th U.S Rock Mechanics/Geomechanics Symposium.

Savalli, L. and Engelder, T., 2005. Mechanisms controlling rupture shape during subcritical growth of joints in layered rocks. Bulletin of the Geological Society of America, 117(3–4), 436–449.

Scholz, C. H., 2010. A note on the scaling relations for opening mode fractures in rock. Journal of Structural Geology, 32(10), 1485–1487. https://doi.org/10.1016/j.jsg.2010.09.007

Schultz, R. A., 2019. Geologic Fracture Mechanics. In Geologic Fracture Mechanics. Cambridge University Press.

Sharon, E. and Fineberg, J., 1999. Confirming the continuum theory of dynamic brittle fracture for fast cracks. Nature, 397(6717), 333–335.

Shlyapobersky, J. and Chudnovsky, A., 1994. Review of recent developments in fracture mechanics with petroleum engineering applications. Paper SPE 28074 Presented at the Eurock SPE/ISRM Rock Mechanics in Petroleum Engineering Conference, 381–389.

Smith, M. B. and Montgomery, C. T., 2015. Hydraulic fracturing (1st ed.). CRC Press.

Spicer, S. and Coenen, E., 2018. Estimation of fracture geometries from poroelastic pressure responses in offset wells. SPE/AAPG/SEG Unconventional Resources Technology Conference 2018, URTC 2018.

Stöckhert, F., 2015. Thesis: Fracture mechanics applied to hydraulic fracturing in laboratory experiments

Suri, Y., Islam, S. Z. and Hossain, M., 2020. Effect of fracture roughness on the hydrodynamics of proppant transport in hydraulic fractures. Journal of Natural Gas Science and Engineering, 80.

van Dam, D. B. and de Pater, C. J., 2001. Roughness of Hydraulic Fractures: Importance of In-SItu Stress and Tip Processes. SPE Journal, 6(1), 4–13.

Webster, P., Cox, B. and Molenaar, M., 2013. Developments in Diagnostic Tools for Hydraulic Fracture Geometry Analysis. Unconventional Resources Technology Conference 2013, URTC 2013.

Wrobel, M., Mishuris, G. and Piccolroaz, A., 2017. Energy release rate in hydraulic fracture: Can we neglect an impact of the hydraulically induced shear stress? International Journal of Engineering Science, 111, 28–51.

Yang, H., Guo, Y., Wang, L., Bi, Z., Guo, W., Zhao, G. and Yang, C., 2022. Study on the Stimulation Effectiveness Evaluation of Large-Scale Hydraulic Fracturing Simulation Experiment Based on Optical Scanning Technology. SPE Journal, 1–19.

Zhang, G., Gutierrez, M. and Chao, K., 2019. Hydrodynamic and mechanical behavior of multi-particle confined between two parallel plates. Advanced Powder Technology, 30(2), 439–450.

Zhang, Q. B. and Zhao, J., 2014. A review of dynamic experimental techniques and mechanical behaviour of rock materials. Rock Mechanics and Rock Engineering, 47(4), 1411–1478.